Int. J. Electrochem. Sci., 17 **(2022)** Article Number: 220652, doi: 10.20964/2022.06.47

International Journal of
ELECTROCHEMICAL
SCIENCE
www.electrochemsci.org

Electroplated Ni-Fe Layer on Stainless Steel Fiber Felt as an Efficient Electrode for Oxygen Evolution Reaction

Bolun Liu, Cen Shen, Luofu Min, Lu Liu, Wen Zhang, Yuxin Wang[*]

State Key Laboratory of Chemical Engineering, Tianjin Key Laboratory of Membrane Science and Desalination Technology, School of Chemical Engineering and Technology, Tianjin University, Tianjin 300072, China
[*]E-mail: yxwang@tju.edu.cn

Received: 2 March 2022 / *Accepted:* 12 April 2022 / *Published:* 7 May 2022

The development of inexpensive and superior electrodes for oxygen evolution reaction (OER) is critical for producing hydrogen by water electrolysis. In this paper, we compare stainless steel fiber felt (SSF), nickel foam (NF) and knitted nickel mesh (NM) as substrates of oxygen evolution reaction (OER) electrodes and use the method of galvanostatic electroplating to prepare a Ni-Fe layer on different substrates. The obtained Ni Fe @SSF electrode with the uniform alloy layer on the surface not only exhibits excellent OER activity (over potential of 250 mV at 10 $mA \cdot cm^{-2}$), but also possesses good stability in 1 M KOH. The Ni Fe @SSF electrode shows potential as an efficient OER electrode in alkaline water electrolysis.

Keywords: Oxygen evolution reaction; Stainless steel fiber felt; Nickel foam; Nickel mesh; Electroplating.

1. INTRODUCTION

It is known that the large-scale use of nonrenewable fossil energy resources has led to severe pollution of the environment [1-8]. Therefore, finding and adopting clean and renewable energy resources have become crucial [9]. Solar energy and wind energy are both important renewable energy, but they have transient characteristics, which makes it necessary to convert the generated energy into other media for storage[10]. Hydrogen energy is one of the most ideal energy carriers because of its clean, efficient and high energy density characteristics [11]. Hence, the production of hydrogen has become a main focus in the field of energy research [1]. Among the various methods of hydrogen production, the electrolysis of water has unique advantages, such as convenient utilization of clean and sustainable solar energy, high purity of production and simple operation [12-15].

However, the wide application of water electrolysis still faces some hurdles, including the sluggish dynamics of oxygen evolution reaction (OER) on account of the multi-steps electron transfer

process [16, 17]. In addition, although noble metal oxides such as RuO_2 and IrO_2 show excellent OER performance, their scarcity and high price restrict their economic competitiveness [18]. In contrast, transition metals can also catalyze water electrolysis and have the advantages of low cost, easy availability and good stability [19].

Stainless steel could be an ideal electrode material in water electrolysis because of its main components, Fe, Cr and Ni, all of which have electrocatalytic activity[20]. Furthermore, stainless steel has high mechanical strength, corrosion resistance and excellent electrical conductivity [14, 21, 22]. Zhang et al. [14] reported interconnected MoS_2 nanosheets grown on commercial stainless steel to improve the HER activity. Lyu et al. [20] demonstrated that stainless steel-based electrodes showed an excellent water-splitting performance. Moureaux et al. [23] investigated activated 316 L stainless steel electrodes for OER in KOH electrolyte. Schäfer et al. [24, 25] modified the surface of AISI 304, which showed excellent performance as an OER electrode. The stainless steel plate was rusted through a hydrothermal method and directly activated into a robust OER electrode by electrochemical oxidation–reduction cycle in alkaline electrolyte[26]. Fe Ni LDH@SSF was proved to exhibit remarkable catalytic activities for both OER and HER[27]. Besides, the study of the HER on different stainless steel electrodes in alkaline solutions has been reported[28]. N-doped surface-etched stainless steel and N-P-doped surface-etched stainless steel have been reported to show good electrocatalytic properties toward HER and OER, respectively[29].

This paper studies SSF, NF and NM as substrates of OER electrodes for water electrolysis and modifies different substrates through the galvanostatic electroplating method to obtain the Ni Fe @SSF, the Ni Fe @NF and the Ni Fe @NM, respectively, because of the excellent activity and stability of Ni-Fe catalyst[30]. The effects of electrode substrates were investigated. The influences of electroplating conditions on the electrocatalytic performance of electrodes were also studied. The prepared Ni Fe @SSF electrode exhibits not only outstanding OER performance, but also good stability under alkaline conditions.

2. EXPERIMENTAL

2.1. Chemical reagents and experimental materials

Sulfuric acid (H_2SO_4), anhydrous ethanol (C_2H_6O), potassium hydroxide (KOH), nickel sulfate hexahydrate ($NiSO_4·6H_2O$), ferrous sulfate heptahydrate ($FeSO_4·7H_2O$), boric acid (H_3BO_3), sodium dodecyl sulfate ($C_{12}H_{25}SO_4Na$) and isopropyl alcohol (C_3H_8O) were purchased from Tianjin Kemiou Chemical Reagent Co., Ltd. Iridium powder and Nafion solution (DuPont D520,5%) were bought from Shanghai Hesen Electric Co., Ltd. 316 L-SSF (BZ50D) (Cr: 16.00~18.00%, Ni: 12.00~15.00%, Mo:2.00~3.00%, Mn≤2.00%, Si≤1.00%, P≤0.035%, C≤0.030%, S≤0.030%) was purchased from Kunshan Yinghuixiong Electronic Technology Co., Ltd. NF (110 ppi) was purchased from Suzhou Keshenghe Metal Materials Co., Ltd. N6-NM (200 mesh) was purchased from Conway Wire Mesh Products Co., Ltd. All chemicals were used as received without further purification.

2.2. Electroplating Ni-Fe on substrates

The SSF, NF and NM were all cut into 1.0×1.0 cm^2 pieces with a tab, and sonicated in 0.5 M H_2SO_4 for 30 min, and then washed with deionized water and anhydrous ethanol. The SSF, NF and NM were dried at room temperature and then used as cathodes. A Pt sheet was used as anode. The electroplating solution was composed of nickel sulfate hexahydrate (24 mmol), ferrous sulfate heptahydrate (6 mmol), boric acid (24 mmol) as the buffer agent, sodium dodecyl sulfate (0.2 mmol) as the wetting agent and deionized water (60 mL). The Ni Fe @SSF, the Ni Fe @NF and the Ni Fe @NM were obtained through galvanostatic electroplating for 20 min with the current density of 20 $mA \cdot cm^{-2}$.

2.3. Characterizations

The phase compositions of the as-prepared materials were characterized by X-ray diffraction (XRD) (D8 Focus, Germany Brock AXS Co., Ltd) with 2θ scanned from 10° to 80° at $10° \cdot min^{-1}$. The morphologies of the electrodes were characterized through scanning electron microscopy (SEM) (S-4800, Hitachi of Japan). The element composition of the electrodes was characterized by energy dispersive spectroscopy (EDS) (EDAX, AMETEK).

2.4. Electrochemical measurements

All electrochemical measurements were carried out using a work station (PARSTAT 2273, AMETEK) with a three-electrode system in 1 M KOH. Within the system, the as-prepared materials, Hg/HgO electrode and Pt sheet were used as working electrode, reference electrode and counter electrode, respectively. All the obtained potentials were converted to the reversible hydrogen electrode (RHE) on the basis of the equation: $E_{(RHE)} = E_{(Hg/HgO)} + 0.059pH + 0.098$. Besides, the Ir/SSF electrode was prepared through the method of immersing 1.0×1.0cm^2 SSF in catalyst ink (solution mixed with 400 μL deionized water, 600 μL isopropyl alcohol and 15 μL Nafion solution sonicated for1 h) with a loading of 0.1 $mg \cdot cm^{-2}$. Linear sweep voltammetry (LSV) was carried out with a scan rate of 5 $mV \cdot s^{-1}$, the result of which was corrected with 90% iR compensation. The size of electrochemical active surface area (ECSA) can be demonstrated by the obtained double-layer capacitance (C_{dl}). The Nyquist plot was obtained with frequencies ranging from 100 kHz to 0.1 Hz. The chronopotentiometric test was carried out at 10 $mA \cdot cm^{-2}$ and 100 $mA \cdot cm^{-2}$ for 200 h, respectively.

3. RESULTS AND DISCUSSION

The XRD results of SSF, NF, NM and the corresponding electroplating Ni-Fe decorating materials are shown in Figure 1. The XRD results of the Ni Fe @SSF and the Bare-SSF exhibit similar main peaks located at 43.6°, 50.8° and 74.7° corresponding to the (111), (200) and (220) facets

of austenitic steel , respectively (PDF card no. 33-0397). In contrast, the strength of peaks of the Ni Fe @SSF is weaker than the Bare-SSF due to the exotic Ni-Fe plating layer on the SSF.

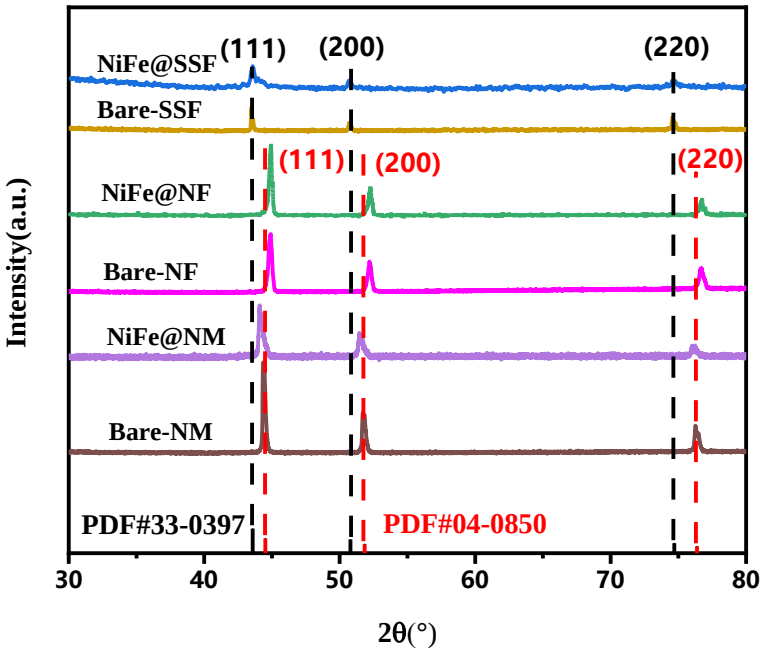

Figure 1. XRD patterns of the Ni Fe @SSF, the Bare-SSF, the Ni Fe @NF, the Bare-NF, the Ni Fe @NM and the Bare-NM.

a

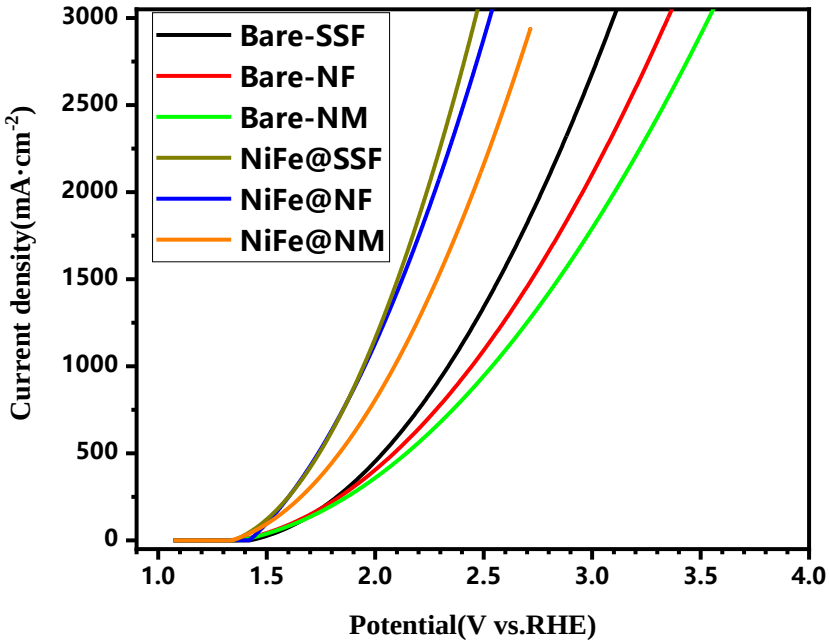

b

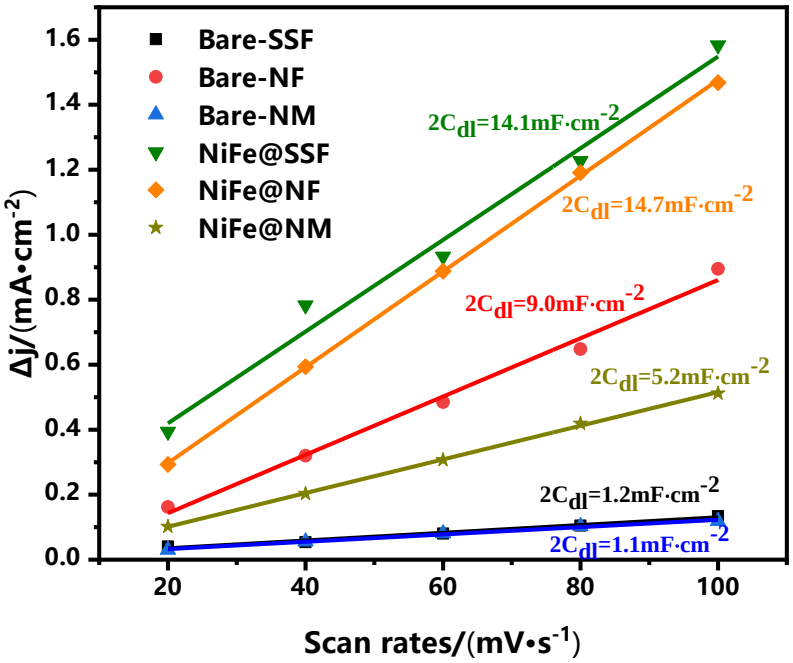

Figure 2. (a) LSV curves of Bare-SSF, Bare-NF, Bare-NM, Ni Fe @SSF, Ni Fe @NF and Ni Fe @NM for OER in 1 M KOH (with 90% iR compensation). (b) C_{dl} plots of Bare-SSF, Bare-NF, Bare-NM, Ni Fe @SSF, Ni Fe @NF and Ni Fe @NM.

Besides, the XRD patterns of the Ni Fe @NF,the Bare-NF, the Ni Fe @NM and the Bare-NM exhibit similar main peaks located at 44.5°, 51.8° and 76.4° corresponding to the (111), (200) and (220) facets of nickel, respectively (PDF card no. 04-0850). Compared with the Bare-NF and the Bare-NM, the main peaks of the Ni Fe @NF and the Ni Fe @NM shift to lower angles on account of the introduction of the larger iron atom [31].

The LSV curves and C_{dl} curves measured for Bare-SSF, Bare-NF, Bare-NM, Ni Fe @SSF, Ni Fe @NF and Ni Fe @NM for OER in 1 M KOH are shown in Figure 2 a and b, respectively. What can be seen from the Figure 2 a is that the electrochemical performances of the Ni-Fe electroplated electrodes are all better than the pristine samples. At current densities higher than 1500 $mA \cdot cm^{-2}$, the performance of the Ni Fe @SSF surpasses the Ni Fe @NF. From Figure 2 b, we can see that the C_{dl} of the Ni Fe @SSF is approximately 12 times as large as the C_{dl} of the Bare-SSF. Whereas the C_{dl} of the Ni Fe @NF is not more than twice as large as the C_{dl} of the Bare-NF and the C_{dl} of the Ni Fe@ NM is approximately 5 times as large as the C_{dl} of the Bare-NM. From what has been discussed above, we can see that the relationship of C_{dl} values of different samples can explain the relationship of electrochemical performances shown in LSV curves (i.e., the greater the C_{dl} value, the better the electrochemical performance). However, compared with the Ni Fe @NF and the Bare-NF, the Ni Fe @SSF and the Bare-SSF show better electrochemical performances, respectively, although the C_{dl} values of the Ni Fe @NF and the Bare-NF are greater. The result indicates that compared with NF, the intrinsic activity of the active site of SSF is better.

Table 1. The electroplating conditions of different samples

	Ni Fe@SSF-1	Ni Fe@SSF-2	Ni Fe@SSF-3	Ni Fe@SSF-4	Ni Fe@SSF-5	Ni Fe@SSF-6
Current density	20	20	20	20	10	30
Electroplating time (min)	10	20	30	40	20	20

The influence of the electroplating time and the current density were both investigated. The electroplating time was set to 10 min, 20 min, 30 min and 40 min, and the current density was set to 10 $mA \cdot cm^{-2}$, 20 $mA \cdot cm^{-2}$ and 30 $mA \cdot cm^{-2}$. The electroplating conditions of different samples are shown in Table 1. As shown in Figure 3 a-b and i-j, the electroplating layers on the surface of Ni Fe@SSF-1 and Ni Fe@SSF-5 are uneven. Moreover, cracks can be observed on the electroplating layers in Figure 3 e-h and k-l. In a word, a too short electroplating time and too small current density results in an uneven distribution of the Ni-Fe electroplated layer, and a too long electroplating time and too large current density results in the appearance of cracks on the electroplated layers.

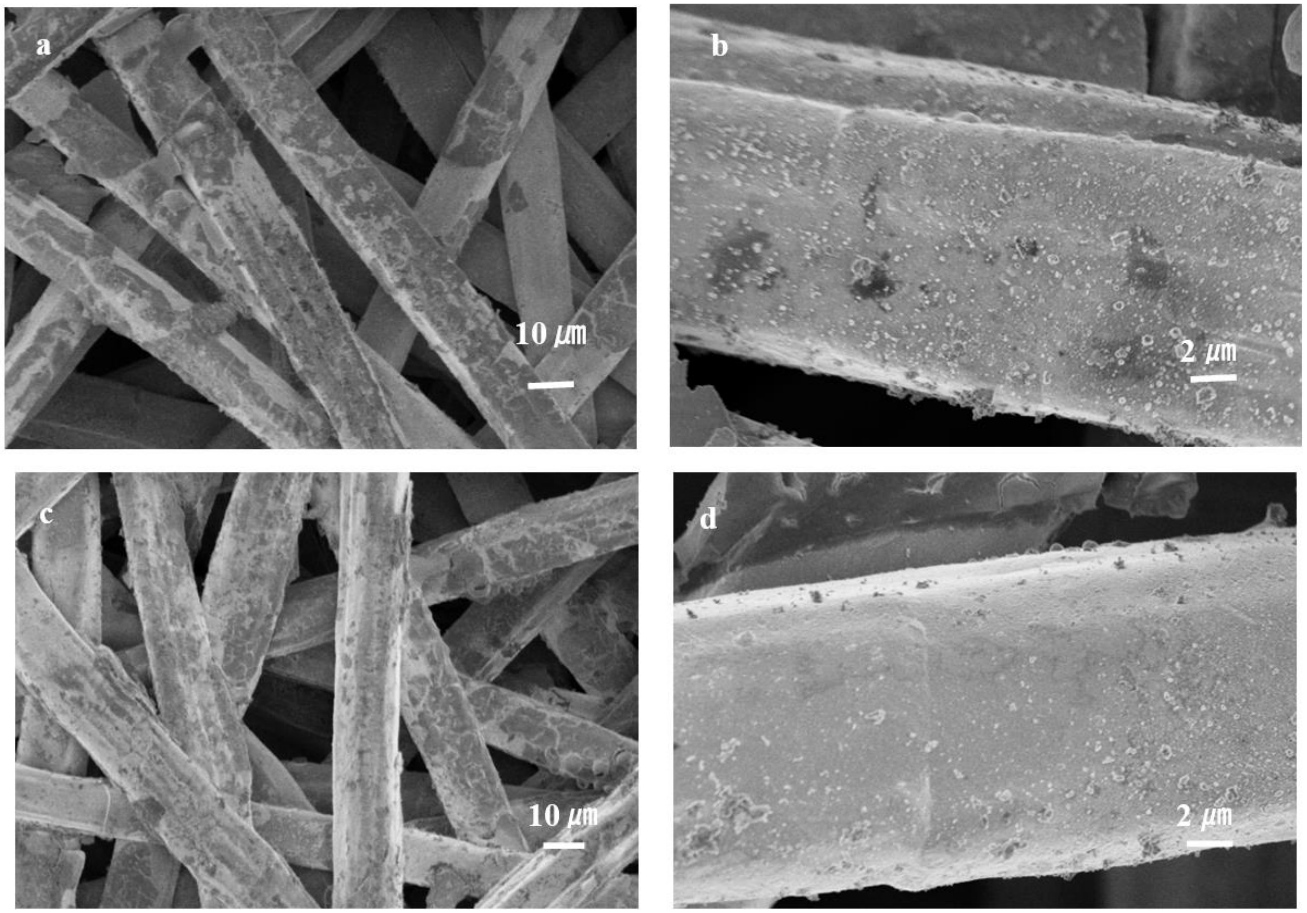

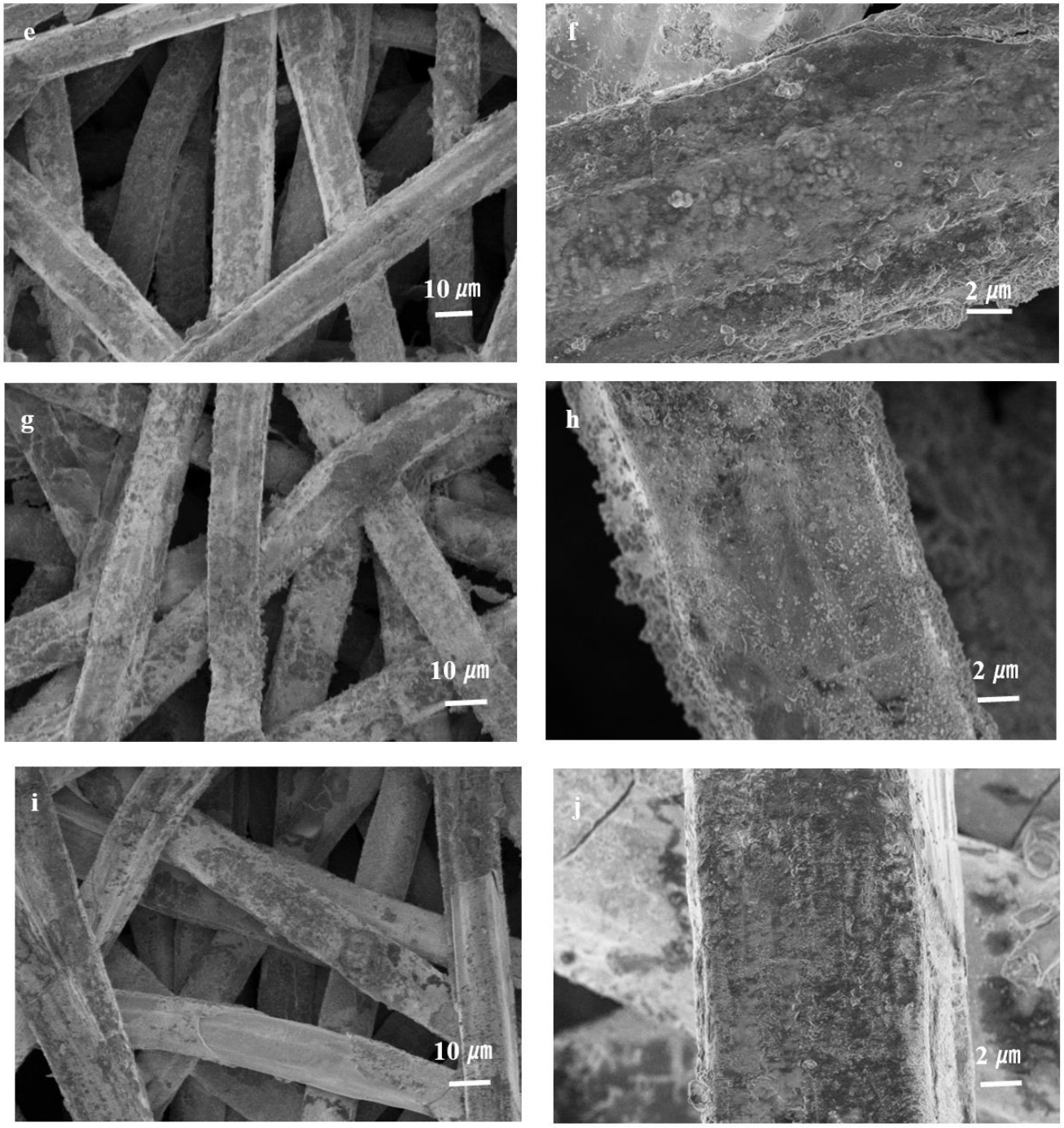
e
10 μm
f
2 μm
g
10 μm
h
2 μm
i
10 μm
j
2 μm

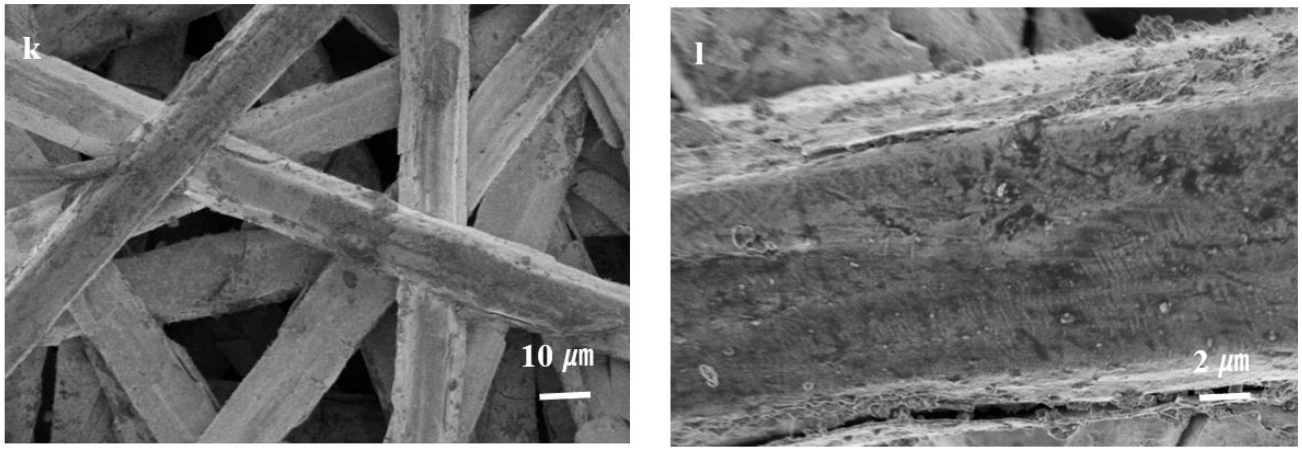

Figure 3. SEM images of (a, b) Ni Fe@SSF-1, (c, d) Ni Fe@SSF-2, (e, f) Ni Fe@SSF-3, (g, h) Ni Fe@SSF-4, (i, j) Ni Fe@SSF-5, (k, l) Ni Fe@SSF-6

Table 2. The atomic ratios of different samples obtained by EDS

	Bare - SSF	Ni Fe@SSF-1	Ni Fe@SSF-2	Ni Fe@SSF-3	Ni Fe@SSF-5	Ni Fe@SSF-6
Mo L (%)	1.14	0.15	0.09	0.02	0.49	0.20
Cr K (%)	18.90	4.92	2.90	2.01	16.77	8.21
Mn K (%)	0.38	0.34	0.24	0.46	0.58	0.31
Fe K (%)	68.98	45.43	41.51	44.82	61.07	55.27
Ni K (%)	10.59	49.17	55.25	52.69	21.09	36.00

Figure 4. (a) SEM image of Ni Fe@SSF-2 and the corresponding elemental color maps of (b) Fe element and (c) Ni element.

Table 2 shows the element compositions of different samples, which manifest that the total content of Fe element and Ni element clearly increases, estimating the successfully prepared Ni-Fe layer on the SSF. From Figure 4 a-c, we can see that the distribution of Fe element and Ni element is uniform on the surface of Ni Fe @SSF. In conclusion, the electrodes which present similar content of Fe element and Ni element possess a complete and uniform electroplated layer.

As shown in Figure 5 a, the OER performance of the Ni Fe @SSF is better than the Ir/SSF. The over potential at 10 $mA \cdot cm^{-2}$ of Ni Fe @SSF-2 is only 250 mV, which is lower than the value of 310 mV of the Ir/SSF. From Figure 5 b, we can see that the Tafel slope of the Ni Fe @SSF is smaller than

that of the Bare-SSF and the Ir/SSF, which indicates the Ni Fe @SSF has better OER kinetic activity. The Nyquist plots are shown in Figure 5 c, from which we can see that the Ni Fe @SSF possesses a lower charge transfer resistance than Bare-SSF.

Compared with similar electrode materials reported in other papers, the performance of the Ni Fe @SSF electrode is competitive.The comparison of the Ni Fe @SSF electrode with other similar electrode materials is represented in Table 3. From Table 3, it can be seen that the values of the over potential and the Tafel slope for the Ni Fe @SSF electrode are both low, which indicates the superior performance of the Ni Fe @SSF electrode.

Table 3. Comparison of the performance of different electrode materials for oxygen evolution reaction

Electrocatalyst	Electrolyte	Over potential (mV)	Tafel slope (mV·dec-1)	Ref
NiFe-LDH@NiFe-Bi/CC	1 M KOH	294@50 mA·cm^{-2}	96	[32]
NiFe Oxide@NF	1 M KOH	255@10 mA·cm^{-2}	55	[33]
Ni/CoFe2O4	1 M KOH	416@100 mA·cm^{-2}	47	[34]
NiFeCH(Ce)	1 M KOH	252@100 mA·cm^{-2}	59	[35]
NiFe2O4/NiFe (OH)x	1 M KOH	276@10 mA·cm^{-2}	68	[36]
Ni Fe @SSF	1 M KOH	250@10 mA·cm^{-2}	17	This work

a

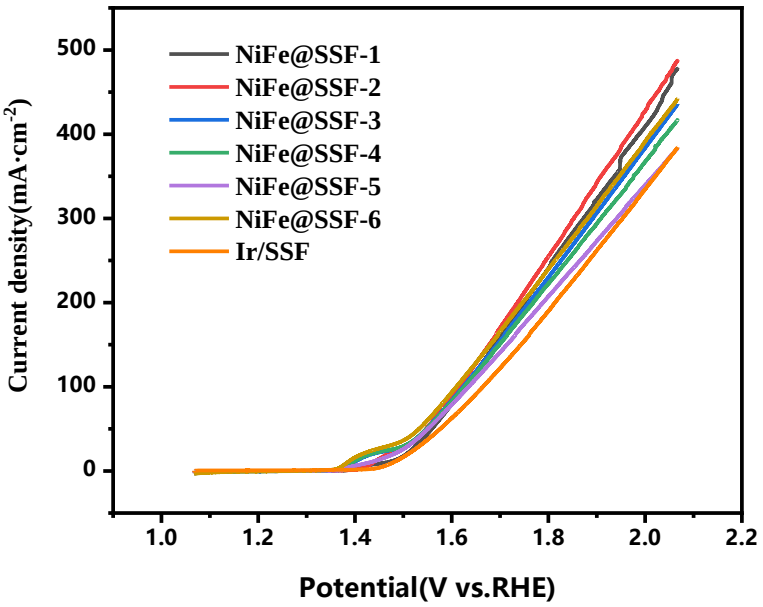

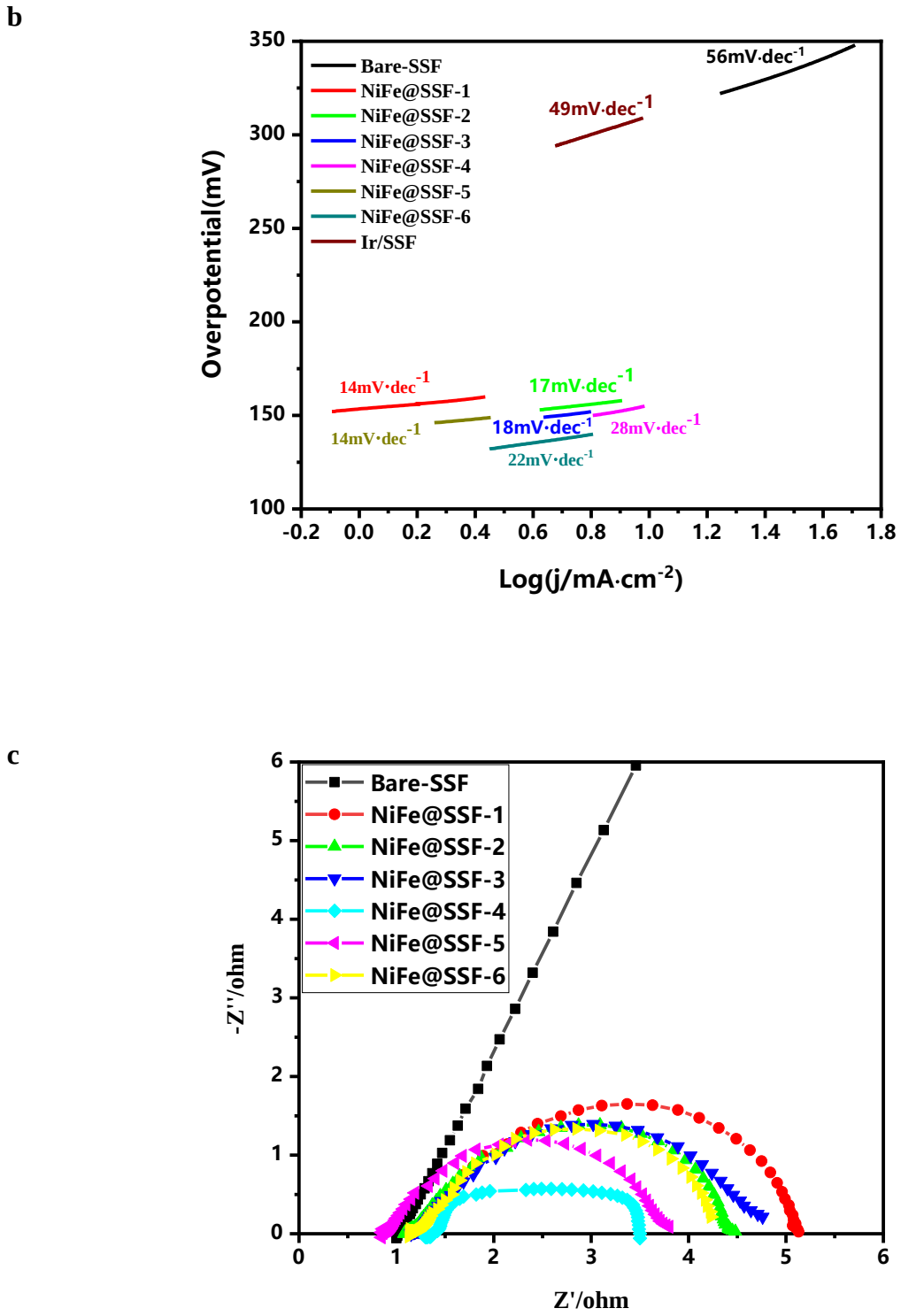

Figure 5. (a) LSV curves of different Ni Fe @SSF and Ir/SSF. (b) Tafel plots of Bare-SSF, different Ni Fe @SSF and Ir/SSF. (c) Nyquist plots of Bare-SSF and different Ni Fe @SSF.

To measure the stability of the Ni Fe @SSF electrode, a chronopotentiometric test was conducted in 1 mol·L^{-1} KOH at current densities of 10 mA·cm^{-2} and 100 mA·cm^{-2}. The results are shown in Figure 6. According to Figure 6, the Ni Fe @SSF exhibits good stability at current densities of 10 mA·cm^{-2} and 100 mA·cm^{-2}. During the 200 h electrolysis process, the potential only increases by

11 mV and 23 mV at current densities of 10 mA·cm^{-2} and 100 mA·cm^{-2}, respectively. In a word, the Ni Fe @SSF can be applied as an OER electrode under alkaline conditions for an extended period of time.

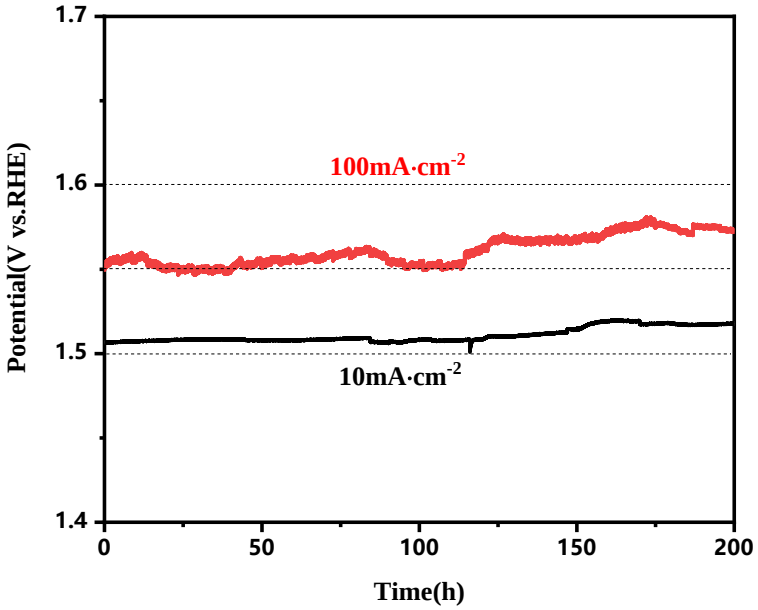

Figure 6. Chronopotentiometric curves of Ni Fe@SSF-2 at current densities of 10 mA·cm^{-2} and 100 mA·cm^{-2} in 1 mol·L^{-1} KOH at room temperature.

4. CONCLUSIONS

In summary, SSF is compared with NF and NM, and the results indicate that SSF shows potential as the substrate of an OER electrode in alkaline situations due to its lower over potential at large current densities and large ECSA. The Ni Fe @SSF electrode obtained through the method of galvanostatic electroplating exhibits superior electrochemical performance. The over potential of the Ni Fe@SSF-2 is only 250 mV at 10 mA·cm^{-2}, which is lower than the Ir/SSF. The Ni-Fe electroplated layer formed on Ni Fe@SSF-2 is uniform. Besides, the Ni Fe@SSF-2 has a low Tafel slope and a small charge transfer resistance, suggesting its superior kinetics toward OER. Furthermore, the Ni Fe@SSF-2 also possesses good stability at 10 mA·cm^{-2} and 100 mA·cm^{-2}, with potential increments of only 11 mV and 23 mV, respectively, observed during a 200 h chronopotentiometric test. In a word, SSF is a good choice as a substrate, and the electroplating of a Ni-Fe alloy layer onto the substrate offers a good method to improve the performance of electrodes for OER in alkaline water electrolysis.

ACKNOWLEDGMENTS
The authors acknowledge the financial support of Tianjin University towards the open access of this research work.

References

1. S. Zhu, C. Chang, Y. Sun, G. Duan, Y. Chen, J. Pan, Y. Tang and P. Wan, *International Journal of Hydrogen Energy*, 45 (2020) 1810.
2. J. S. Chen, J. Ren, M. Shalom, T. Fellinger and M. Antonietti, *ACS Appl. Mater. Interfaces*, 8 (2016) 5509.
3. C. Yuan, H. B. Wu, Y. Xie and X. W. D. Lou, *Angew. Chem. Int. Ed*., 53 (2014) 1488.
4. H. Tang, S. Cai, S. Xie, Z. Wang, Y. Tong, M. Pan and X. Lu, *Adv. Sci.*, 3 (2016) 1500265.
5. M. Lee, M. S. Jee, S. Y. Lee, M. K. Cho, J. Ahn, H. Oh, W. Kim, Y. J. Hwang and B. K. Min, *ACS Appl. Mater. Interfaces*, 10 (2018) 24499.
6. R. A. Senthil, J. Pan, X. Yang and Y. Sun, *International Journal of Hydrogen Energy*, 43 (2018) 21824.
7. M. N. Uddin and W. M. A. W. Daud, *Energy Fuels*, 28 (2014) 4300.
8. U. Sikander, S. Sufian and M. A. Salam, *International Journal of Hydrogen Energy*, 42 (2017) 19851.
9. K. C. Leonard, M. I. Tejedor-Anderson and M. A. Anderson, *International Journal of Hydrogen Energy*, 37 (2012) 18654.
10. J. Chi and H. Yu, *Chinese Journal of Catalysis*, 39 (2018) 390.
11. A. Kazim and T. N. Veziroglu, *RENEW ENERG*, 24 (2001) 259.
12. A. Yilanci, I. Dincer and H. K. Ozturk, *Progress in Energy and Combustion Science*, 35 (2009) 231.
13. P. K. Dubey, A. S. K. Sinha, S. Talapatra, N. Koratkar, P. M. Ajayan and O. N. Srivastava, *International Journal of Hydrogen Energy*, 35 (2010) 3945.
14. K. Zhang, Y. Liu, B. Wang, F. Yu, Y. Yang, L. Xing, J. Hao, J. Zeng, B. Mao, W. Shi and S. Yuan, *International Journal of Hydrogen Energy*, 44 (2019) 1555.
15. M. G. Walter, E. L. Warren, J. R. Mckone, S. W. Boettcher, Q. Mi, E. A. Santori and N. S. Lewis, *Chem. Rev*., 110 (2010) 6446.
16. H. Dau, C. Limberg, T. Reier, M. Risch, S. Roggan and P. Strasser, *ChemCatChem*, 2 (2010) 724.
17. S. Shiva Kumar and V. Himabindu, *Materials Science for Energy Technologies*, 2 (2019) 442.
18. Y. Shi and B. Zhang, *Chemical Society reviews*, 45 (2016) 1529.
19. Y. Li, M. Zhao, Y. Zhao, L. Song and Z. Zhang, *Part. Part. Syst. Charact*., 33 (2016) 158.
20. Y. Lyu, R. Wang, L. Tao, Y. Zou, H. Zhou, T. Liu, Y. Zhou, J. Huo, S. P. Jiang, J. Zheng and S. Wang, *Applied Catalysis B: Environmental*, 248 (2019) 277.
21. F. Yu, F. Li and L. Sun, *International Journal of Hydrogen Energy*, 41 (2016) 5230.
22. L. Li, V. Breedveld and D. W. Hess, *ACS Appl. Mater. Interfaces*, 4 (2012) 4549.
23. F. Moureaux, P. Stevens, G. Toussaint and M. Chatenet, *Applied Catalysis B: Environmental*, 258 (2019) 117963.
24. H. Schäfer, S. Sadaf, L. Walder, K. Kuepper, S. Dinklage, J. Wollschläger, L. Schneider, M. Steinhart, J. Hardege and D. Daum, *ENERG ENVIRON SCI*, 8 (2015) 2685.
25. H. Schäfer, S. M. Beladi-Mousavi, L. Walder, J. Wollschläger, O. Kuschel, S. Ichilmann, S. Sadaf, M. Steinhart, K. Küpper and L. Schneider, *ACS Catal*., 5 (2015) 2671.
26. H. Zhong, J. Wang, F. Meng and X. Zhang, *Angew. Chem. Int. Ed*., 55 (2016) 9937.
27. L. Wang, X. Huang, S. Jiang, M. Li, K. Zhang, Y. Yan, H. Zhang and J. M. Xue, *ACS Appl. Mater. Interfaces*, 9 (2017) 40281.
28. J. M. Olivares-Ramírez, M. L. Campos-Cornelio, J. Uribe Godínez, E. Borja-Arco and R. H. Castellanos, *International Journal of Hydrogen Energy*, 32 (2007) 3170.
29. M. Balogun, W. Qiu, Y. Huang, H. Yang, R. Xu, W. Zhao, G. Li, H. Ji and Y. Tong, *Adv. Mater*., 29 (2017) 1702095.
30. J. Landon, E. Demeter, N. 0noğlu, C. Keturakis, I. E. Wachs, R. Vasić, A. I. Frenkel and J. R. Kitchin, *ACS Catal*., 2 (2012) 1793.
31. D. Li, M. Koike, L. Wang, Y. Nakagawa, Y. Xu and K. Tomishige, *ChemSusChem*, 7 (2014) 510.

32. L. Zhang, R. Zhang, R. Ge, X. Ren, S. Hao, F. Xie, F. Qu, Z. Liu, G. Du, A. M. Asiri, B. Zheng and X. Sun, *Chem. Eur. J.*, 23 (2017) 11499.
33. B. Li, *Int. J. Electrochem. Sci.*, 14 (2019) 4878.
34. N. Kumar Singh, *Int. J. Electrochem. Sci.*, 15 (2020) 6605.
35. J. Cai, J. Huang, S. Xu, L. Yuan, X. Huang, Z. Huang and C. Zhang, *J Solid State Electrochem*, 23 (2019) 3449.
36. L. Yao, Z. Geng, W. Zhang, X. Wu, J. Liu, L. Li, X. Wang, X. Hou, K. Xu, K. Huang and S. Feng, *ACS Sustainable Chem. Eng.*, 8 (2020) 17194.